

University of Mississippi

eGrove

Honors Theses


Honors College (Sally McDonnell Barksdale
Honors College)

Spring 5-9-2020

Comparison of the Vibrational Modes of Thiolated Gold Nanoparticles Undergoing Core-Conversions Via Raman Spectroscopy

William Gregory Cannella Jr.
University of Mississippi

Follow this and additional works at: https://egrove.olemiss.edu/hon_thesis

 Part of the [Analytical Chemistry Commons](#), [Atomic, Molecular and Optical Physics Commons](#), [Inorganic Chemistry Commons](#), and the [Physical Chemistry Commons](#)

Recommended Citation

Cannella, William Gregory Jr., "Comparison of the Vibrational Modes of Thiolated Gold Nanoparticles Undergoing Core-Conversions Via Raman Spectroscopy" (2020). *Honors Theses*. 1383.
https://egrove.olemiss.edu/hon_thesis/1383

This Undergraduate Thesis is brought to you for free and open access by the Honors College (Sally McDonnell Barksdale Honors College) at eGrove. It has been accepted for inclusion in Honors Theses by an authorized administrator of eGrove. For more information, please contact egrove@olemiss.edu.

**Comparison of the Vibrational Modes of Thiolated Gold Nanoparticles
Undergoing Core-Conversions Via Raman Spectroscopy**

By
William Gregory Cannella, Jr.

A thesis submitted to the faculty of The University of Mississippi in partial fulfillment of
the requirements of the Sally McDonnell Barksdale Honors College.

Oxford, Mississippi
May 2020

Approved by

Advisor: Professor Nathan Hammer

Reader: Professor Amal Dass

Reader: Professor Murrell Godfrey

© 2020

William Gregory Cannella Jr.

ALL RIGHTS RESERVED

ACKNOWLEDGEMENTS

I am amazed by the opportunities presented to me by the University of Mississippi and am grateful for the ability to express my goals and capabilities as a chemist. I would like to thank my parents, Greg and Karen Cannella, and my sister, Natalie Cannella, as well as my friends for their continuous support and love throughout the entirety of my college career. None of my achievements would have been possible without your inspiration and guidance. Furthermore, I would like to thank the Hammer Group, particularly Austin Dorris and Cameron Smith for aiding and mentoring me during my time in the lab. I also thank previous Hammer Group member, Lemuel Tsang, for his consultation and inspiring me to pursue this subject. I thank my advisor, Dr. Kerri Scott, for her guidance and constant support and valuable insight throughout the entirety of my college career, providing me with every opportunity to better myself as a chemist. I would like to thank my thesis advisor, Dr. Nathan Hammer, for his endless advice, hospitality, motivation, and expectations that drove me to become the chemist I am today. Finally, I kindly thank the Dass Group for their continued collaboration and Senthil Eswaramoorthy who provided us with samples of $\text{Au}_{38}(\text{2-PET})_{24}$ and $\text{Au}_{30}(\text{S-tBu})_{18}$.

ABSTRACT

WILLIAM GREGORY CANNELLA, JR.: Characterizing the Vibrational Modes of Thiolated Gold Nanoparticles Undergoing Core-Conversions Via Raman Spectroscopy
(Under the direction of Dr. Nathan Hammer)

In this project, the vibrational characteristics/vibrational modes are explored via Raman Spectroscopy for thiolated-gold nanoparticles. This class of compounds is also known as gold nanoparticles (AuNPs). They remain of great interest in research areas such as catalysis, gold dependent nanoelectronics, drug delivery, and sensing, due to their unique size-dependent optical, chiroptical, and electronic properties. Vibrational spectroscopy of thiolated gold nanoparticles are oftentimes considered nontrivial as the compounds strongly absorb light in the visible region of the electromagnetic spectrum, are generally considered weak scatterers, and give off large amounts of fluorescence. This combined with their black appearance, susceptibility to localized heating, and lack of topographical features makes these compounds challenging to study. These compounds possess unique structural compositions as they are composed of a number of covalently bonded gold atoms forming what is referred to as a gold core complex. This core complex is then surrounded by various gold-thiolate staple molecules such as monomeric (SR-Au-SR), dimeric (SR-Au-SR-Au-SR), trimeric (SR-Au-SR-Au-SR-Au-SR), as well as bridging thiols. Furthermore, the core complex is also surrounded by various ligand groups. For the purposes of this study, the ligands of 2-Phenylethylthiol and *tert*-butylthiol were investigated. One of the biggest opportunities AuNPs provide, is the ability to undergo core-size conversions due to electronic and steric effects of the ligands and the interaction of Au-S bonds. Here, the gold thiolate molecule $\text{Au}_{38}(\text{2-PET})_{24}$ undergoes a core-size reduction via etching with *tert*-butylthiol to produce $\text{Au}_{30}(\text{S-tBu})_{18}$, coined “green-gold” by the Dass Group. Oftentimes, subtle spectral differences are observed between core-size

conversions; however, this study also explores the vibrational spectroscopic changes induced by ligand exchanges for a compound that has yet to be vibrationally studied elsewhere.

TABLE OF CONTENTS

<i>Acknowledgements</i>	<i>iii</i>
<i>Abstract</i>	<i>iv</i>
<i>List of Figures</i>	<i>viii</i>
Chapter 1: Light & Spectroscopy	1
1.1 Nature of Light Overview.....	1
1.2 Generalities of Spectroscopy.....	2
1.2.1 Characteristic Emissions & Quantum States.....	2
1.2.2 The Interaction of Light & Matter.....	3
Chapter 2: Raman Spectroscopy	4
2.1 Raman Spectroscopy Background.....	4
2.2 Light Scattering Phenomena.....	4
2.3 Raman Spectrometer Components & Functionality.....	6
2.3.1 Vibrational Spectroscopy Selection Rules.....	6
2.3.2 Raman Spectrometer Data Collection.....	7
2.3.3 Raman Spectroscopy Versatility & Stokes/Anti-Stokes Shift.....	8
Chapter 3: Thiolated Gold Nanoparticles (AuNPs)	9
3.1 AuNP Class Characteristics & Applications.....	9
3.2 Vibrational Spectroscopy of AuNPs.....	10
3.2.1 Raman Vibrational Spectroscopy of AuNPs.....	10
3.2.2 IR Vibrational Spectroscopy of AuNPs.....	11
3.3 AuNP Core-Conversions.....	12

3.4 Geometric & Energetic Comparison of Au ₃₈ (2-PET) ₂₄ and Au ₃₀ (S-tBu) ₁₈	13
Chapter 4: Raman Spectroscopic Comparison of Au₃₈(2-PET)₂₄ and Au₃₀(S-tBu)₁₈	15
4.1 Introduction.....	15
4.2 Methods.....	16
4.3 Results & Discussion.....	18
4.4 Summary.....	24
Chapter 5: Supplemental Information.....	25
5.1 Experimental Setup & Methodologies.....	25
List of References.....	28

LIST OF FIGURES

Figure 1.1 The Electromagnetic Spectrum.....	3
Figure 2.1 Stokes & Anti-Stokes Shifts.....	4
Figure 2.2 Virtual State Representation of Stokes Shift.....	5
Figure 3.1 Au ₃₈ (2-PET) ₂₄ Core-Size Reduction to Au ₃₀ (S- <i>t</i> Bu) ₁₈	12
Figure 4.1 Au ₃₈ (2-PET) ₂₄ 633 nm Excitation from 100 – 1250 cm ⁻¹	17
Figure 4.2 Au ₃₈ (2-PET) ₂₄ 633 nm Excitation from 175 – 375 cm ⁻¹	17
Figure 4.3 Au ₃₈ (2-PET) ₂₄ 633 nm Excitation from 600 – 900 cm ⁻¹	18
Figure 4.4 Au ₃₈ (2-PET) ₂₄ 633 nm Excitation from 960 – 1060 cm ⁻¹	18
Figure 4.5 Au ₃₀ (S- <i>t</i> Bu) ₁₈ 633 nm Excitation from 50 – 1300 cm ⁻¹	19
Figure 4.6 Au ₃₀ (S- <i>t</i> Bu) ₁₈ 633 nm Excitation from 150 – 350 cm ⁻¹	19
Figure 4.7 Au ₃₀ (S- <i>t</i> Bu) ₁₈ 633 nm Excitation from 575– 700 cm ⁻¹	20
Figure 4.8 Au ₃₀ (S- <i>t</i> Bu) ₁₈ 633 nm Excitation from 900 – 1100 cm ⁻¹	20
Figure 4.9 Au ₃₀ (S- <i>t</i> Bu) ₁₈ 633 nm Excitation from 1100 – 1300 cm ⁻¹	21
Figure 4.10 Au ₃₈ (2-PET) ₂₄ /Au ₃₀ (S- <i>t</i> Bu) ₁₈ Spectral Comparison from 50 – 1250 cm ⁻¹ ...	21
Figure 5.10 Spectral Comparison of Fresh & Degraded Au ₃₀ (S- <i>t</i> Bu) ₁₈ Samples	25

Chapter 1: Light & Spectroscopy

1.1 Nature of Light Overview

In order to understand the functionality of the electromagnetic spectrum as an analytical tool, one must understand the nature of light. Light is oftentimes referred to as a series of photons or a quanta packet or particle of light. A photon is the energy of light described as a single point, this is known as the *wave function collapse*. This description demonstrates that light behaves both as a wave and a particle depending on the experiment used to observe the phenomena.¹ This is commonly referred to as *wave-particle duality* suggested by Max Plank, Louis de Broglie, Albert Einstein and other influential scientists.² Additionally, if light is confined into a single plane, plane polarized light will have an oscillating electric field as well as an oscillating magnetic field, both of which oscillate at 90-degree angles from one another.¹ The idea of electromagnetic waves was postulated by James Clerk Maxwell and later confirmed by Heinrich Rudolf Hertz.² Maxwell postulated light behaved like an electromagnetic wave due to the speed of the electromagnetic wave predicted matching the measured speed of light.² There are several characteristics of light that are extremely important in spectroscopy. Light can travel as single wavelengths, known as monochromatic light, and in multiple wavelengths, known as polychromatic light. The power or intensity of light is a measure of the energy in a given area per second.¹ Wavelength is the distance between the peaks of light oscillations, also known as a period in trigonometric terms. Lower wavelengths will indicate that the light is undergoing more frequent oscillations and is described as having a higher energy than light of less frequent oscillations; therefore, this light will appear as higher energy light on the electromagnetic spectrum than higher wavelength light. These more frequent oscillations, or lower wavelength light will be able to more easily induce higher quantum energy transitions such

as vibrational and electronic transitions than lower energy transitions such as translational and rotational.³⁻⁸ These properties are all interrelated and can be expressed in several equations denoted in Equation 1.1.

$$E = h\nu = \frac{hc}{\lambda} \quad (1.1)$$

1.2 Generalities of Spectroscopy

1.2.1 Characteristic Emissions & Quantum States

Spectroscopy is a class of analytical techniques based on the interaction of light and matter. Using this, scientists can probe the differences in energy levels between quantum states. All atoms and molecules exist in discrete energy states; however, these states are dependent on the molecule's configuration and conformation. By observing these quantum states, we can utilize quantum mechanics to rationalize the results and understand the unique properties of specific systems.³⁻⁸ This is why specific compounds yield characteristic absorption wavelengths and emission spectrums, allowing discrimination between different elements and compounds.

The hierarchy of quantum states can be summarized as intermediates of the ground state and a series of excited states. The specific excitation gives rise to energy transitions characterized as translational, rotational, vibrational, and electronic transitions. These energy transitions parallel the energy increase witnessed in the electromagnetic spectrum, ranging from radio-waves to gamma radiation illustrated in Figure 1.1.

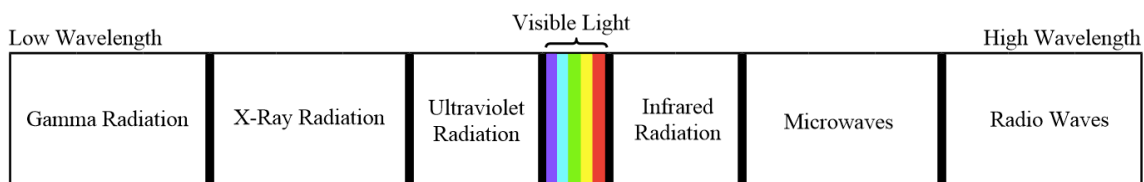


Figure 1.1 Visual aid for the wavelength relationship of the electromagnetic spectrum.

1.2.2 The Interaction of Light & Matter

Understanding the properties of light is just as important as understanding how these properties interact with matter. When light interacts with a molecule it can be *absorbed*, resulting in an overall increase in energy of the molecule. Furthermore, the light can be *transmitted* in which, there is no interaction with the molecule. Light can be *reflected*, causing some light to ‘bounce’ back depending on the refractive index of the material being studied. *Refraction* occurs as light passes through different mediums, changing the speed of that light due to the properties of the material; such as the image distortion we see in water. Additionally, waves of light can *diffuse* around objects that can allow for data collection such as diffraction patterns. Finally, light can undergo *scattering*. There are a variety of scattering processes that result in directional changes in light following collisions with small particles. These interactions allow for the use of a multitude of spectroscopic techniques such as: UV-Vis, Infrared analysis, Nuclear Magnetic Resonance, Phosphorescence, Atomic Absorption Spectroscopy, Atomic Emission Spectroscopy, X-Ray Fluorescence, and Raman Spectroscopy. There are additional variations on these techniques such as Fourier-Transform Infrared Radiation and Surface Enhanced Raman Spectroscopy (SERS) that alter data collection capabilities.

Chapter 2: Raman Spectroscopy

2.1 Raman Spectroscopy Background

The now known Raman effect was first hypothesized by Austrian physicist Adolf Smekal in 1923,⁹ and later discovered by C.V. Raman and K.S. Krishnan in 1928 and promptly named the Raman effect.¹⁰ This methodology mostly utilizes spontaneous Raman scattering, which occurs when the excited state induces a vibration in the molecule and relaxation to a lower vibration state a photon of different energy is emitted. This is known as both Stokes and Anti-Stokes shifts illustrated in Figure 2.1.³⁻⁸

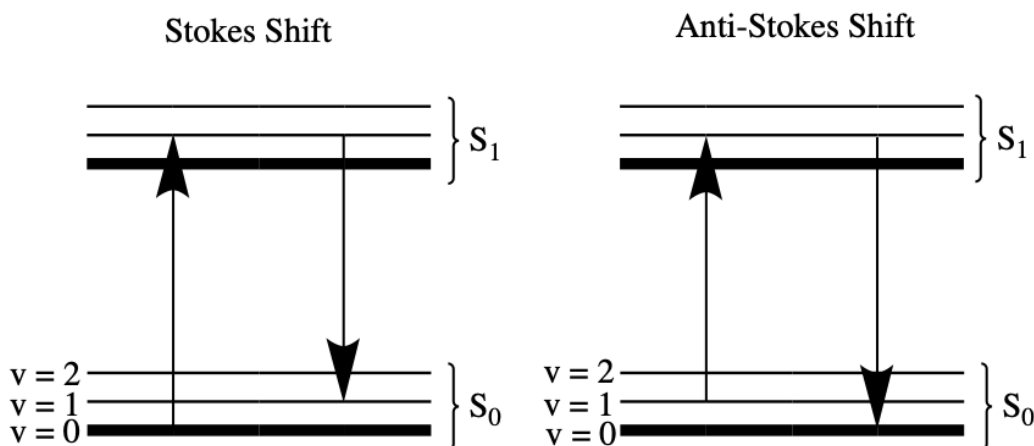


Figure 2.1 Vibrational energy level diagram illustrating the difference in vibrational excitation states of molecules via Stokes and Anti-Stokes shifts.

Some other notable techniques utilize stimulated or resonant Raman scattering, which is essentially when the excited state aligns with the S_1 state, the alternative of which is the creation of a virtual state.

2.2 Light Scattering Phenomena

To further understand Raman spectroscopic techniques, one must understand the variants of light scattering. There are several types of light scattering; these are usually

grouped into elastic and inelastic scattering. Elastic scattering occurs when the incident photon energy striking the molecule has the same photon energy after the collision. This type of scattering is most common in the form of Rayleigh or Mie scattering.^{1, 3-8} This means that the wavelength of scattered light is unchanged from the incident wavelength.³⁻⁸ Furthermore, the scattering effect is impacted by the size of the particle.³⁻⁸ As such, this type of scattering is useful for determining the size and shape of colloids. Raman scattering can also be characterized as Inelastic scattering. Raman scattering is caused by the excitation of a molecule into a higher vibrational state, known as a virtual state.³⁻⁸ It is important to note that the listing as a virtual state occurs if the excitation energy is greater than vibrational transitions but less than necessary to achieve an electronic transition.³⁻⁸ This is illustrated in Figure 2.2.

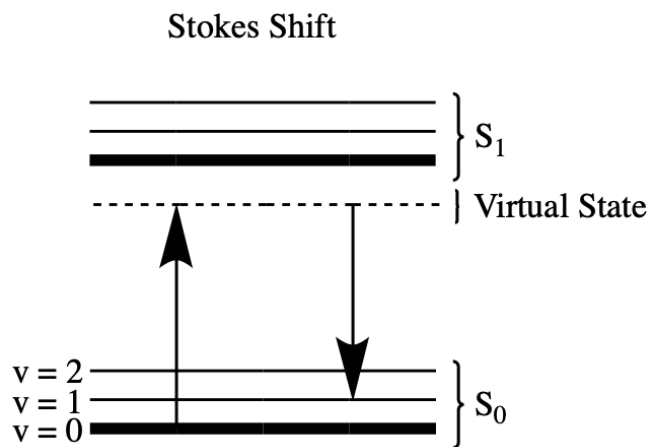


Figure 2.2 Vibrational energy level diagram illustrating a Stokes Shift vibrational excitation via achieved virtual state.

Since these ‘in-between’ states are not quantized, there is effectively an infinite number of achievable excited states for a molecule. This virtual state can be any form of low frequency modes such as vibrational or rotational and is independent of the incident wavelengths. The process of Raman scattering is nearly instantaneous as compared to the lifetime of

fluorescence which can be on the range of picoseconds to milliseconds and nanoseconds respectively.^{3-8, 11} The inelastic scattering of photons causes a change in the energy of the incident photon. This change is viewed as a difference in wavelength from the excitation and detected photons. This phenomenon is utilized in both IR and Raman spectroscopy.

2.3 Raman Spectrometer Components & Functionality

2.3.1 Vibrational Spectroscopy Selection Rules

Raman Spectroscopy utilizes the phenomenon of inelastic light scattering to probe the low frequency modes of atoms and molecules by illuminating samples with a monochromatic light source followed by the collection of scattered light. This process is often considered complementary to IR Spectroscopy as some vibrations are IR active but not Raman active and vice versa. This is due to the difference of selection rules between IR and Raman. IR Spectroscopy requires a change in the dipole moment to be considered 'active' while Raman Spectroscopy requires a molecule to undergo a net change in polarizability. This means a detectable change in electron distribution in response to the applied electric field must occur.¹² These compounds are considered anisotropic while molecules that are not Raman active are considered isotropic. Oftentimes, a lower nuclear charge influence on the surrounding electrons, can cause a greater change in electron density.¹² This can be done by increasing the bond distance and by inducing vibrations.¹² Generally speaking, larger molecules tend to have greater polarizability due to this increased distance of electrons from nuclear charge.¹² These vibrational changes in polarizability are of principle interest for Raman spectroscopy.

2.3.2 Raman Spectrometer Data Collection

The Raman spectrometer functions by shining a radiant source onto the sample, such as helium/neon (633 nm), argon ion (488 nm), krypton ion (532 nm), neodymium/yttrium aluminum garnet (Nd:YAG) (1064 nm), and 785 nm NIR diode lasers.¹³ Following this, the scattered light is collected and progresses through a monochromator, possibly with several gratings, to eliminate Rayleigh scattering and followed by a detector. A variety of detectors are used, ranging from photomultiplier tubes (PMTs), charge injection devices (CIDs), and charge-coupled devices (CCDs) which require cryogenic cooling.¹² Following light scattering, wavelengths collected by the detector that are close to the incident wavelength are filtered out from the final spectrum. All other collected light is processed by a spectrometer, then radiation intensity is converted into an electrical signal via a transducer. The CCD is responsible for storing a photo generated charge in a 2D array and after a given time, the electrons stored are read and produce a signal, resulting in a very sensitive detector with a high signal to noise ratio.¹²⁻¹³ The spectrometer is responsible for separating out scattered light according to the individual wavelengths, and presents this data as a graph displaying an intensity - wavenumber relationship.¹²⁻¹³ Furthermore, on the sample level, the measuring of vibrations occurs by surface plasmon resonance. Surface plasmon resonance occurs when the interface of two surfaces are stimulated by a light source which induces oscillation of electron densities.^{3-8, 13} As such, these can only be generated in the presence of free electrons.^{12, 13} This is why metal is usually a useful surface, effectively inducing electromagnetic waves to the sample surface.¹³

2.3.3 Raman Spectroscopy Versatility & Stokes/Anti-Stokes Shift

Raman Spectroscopy is a very versatile technique partly due to its qualitative and quantitative capabilities. The peaks are unique to the specific bond types of a molecule.¹³ With knowledge of functional groups, spectral behaviors, and the available vibrational states, one can identify specific molecules as well as the type of vibration.^{3-8, 12, 13} Additionally, the intensity of the Raman signal is directly proportional to the concentration of the sample.

Despite the capabilities of Raman spectroscopy, it has some disadvantages. Compared to other light interactions such as fluorescence and phosphorescence, scattered light tends to be much weaker. As such, properly utilizing a Raman spectrometer becomes effectively amplifying or enhancing the intensity of Raman scattered light. When a photon collides with matter, an energy shift occurs, and the incident photon will either have more or less energy than the emitted photon in the inelastic scattering process. This phenomenon is referred to as Stokes and Anti-Stokes shifts respectively.¹³ Raman spectrometers most commonly measure Stokes shifts due to their higher intensity signals; however, anti-Stokes is often useful for fluorescent compounds.¹³ This occurs because Stokes shifts are more common than anti-Stokes, since anti-Stokes requires a molecule to be in a previously excited state, before the incident photon collision.¹³ This can be illustrated with a vibrational energy level diagram located in Figure 2.1. The difference in energy for Stokes and anti-Stokes correspond to vibrational energy transitions.

Chapter 3: Thiolated Gold Nanoparticles (AuNPs)

3.1 AuNP Class Characteristics & Applications

The first thiolate-protected cluster to be crystalized and studied was $\text{Au}_{102}(\text{SR})_{44}$ by Jatzinsky *et al.* in 2007 and was found to have the presence of monomeric and dimeric staple units covering a densely packed gold core.¹⁴ Since then, the study of AuNPs has remained a field of interest for many research opportunities. These staple units play an important role in determining the structure of the Au core, and therefore the molecular properties.¹⁵ These can appear in a variety of forms such as monomeric (SR-Au-SR), dimeric (SR-Au-SR-Au-SR), and trimeric (SR-Au-SR-Au-SR-Au-SR).¹⁶ In addition to these staples, the gold core can also be surrounded by a plethora of structural motifs and various ligand types.¹⁶ The arrangement and structure of the ligand types impact the conformation and the number of gold atoms present within the gold core. This particular class of compounds have a variety of applications such as nanoelectronics, catalysts, drug delivery, and sensing.¹⁵ This is primarily due to the compounds unique size-dependent optical, chiroptical, and electronic properties.¹⁶ Because of these characteristics, it is useful to understand the binding properties of the Au-S interface and investigate the implications of changes in the gold core structure. Furthermore, AuNPs are heavily studied due to their atomic monodispersity, molecular properties,¹⁷⁻¹⁸ stability from geometric¹⁹ and electronic shell closings²⁰ therefore, it is also important to investigate the thiolate-fold interaction for self-assembled monomers (SAMs),²¹ gold nanoparticles and clusters,²² and gold-based molecular electronics.²³

3.2 Vibrational Spectroscopy of AuNPs

3.2.1 Raman Vibrational Spectroscopy of AuNPs

Vibrational spectroscopy is very useful for studying gold clusters as it provides insight into the structure of the Au-S interface. There have been a variety of density functional theory (DFT) calculations in previous works investigating small thiolated clusters that have been used to predict different Far-IR and Raman spectra.²⁴ Research performed by Tlahuice-Flores *et al.* mentions that the calculations predicted a “richer” spectrum for Raman as compared to the far-infrared spectrum.²⁴ This makes Raman spectroscopy a promising technique on the frontier of vibrational spectroscopy of thiolate gold nanoparticles. There have been other promising Raman spectroscopy studies utilizing SERS to enhance the vibrational signals of gold clusters to further investigate their conformational properties. A previous study by Price and Whetten²⁵ and Murray *et al.*²⁶ reported experimental Raman of benzenethiolate protected gold clusters at a time when the structure and size were unknown. Another study performed by Varnholt *et al.* in 2014, engaged in the systematic study of Far-IR spectra of 2-PET protected clusters,¹⁶ while a Heiz & co-workers investigated mid-IR spectra of $[\text{Au}_{25}(\text{2-PET})_{18}]^{0/-}$, $\text{Au}_{38}(\text{2-PET})_{24}$, $\text{Au}_{40}(\text{2-PET})_{24}$, and $\text{Au}_{144}(\text{2-PET})_{60}$.²⁷ Additionally, Varnholt *et al.* investigated the effect of stabilizing ligands on $\text{Au}_{25}(\text{2-PET})_{18-2x} (\text{S-}/\text{rac-BINAS})_x$, $\text{Au}_{25}(\text{CamS})_{18}$, and $\text{Au}_n\text{BINAS}_m$. For reference, BINAS refers to 1,1'-binaphthyl-2,2'-dithiol and CamS refers to 1R,4S-camphorithiol. They reported surface interactions of Au-S-C bending and Au-S radial vibrations that were impacted by the type and number of gold-thiolate binding ligands, therefore influencing the collected spectra.²⁷ Additionally, an undergraduate in the Hammer Lab at the University of Mississippi, Lemuel Tsang, in 2017 investigated the vibrational modes of $\text{Au}_{38}(\text{2-PET})_{24}$ using a temperature control stage at 0 and -100°C

temperatures along with various laser wavelengths and powers. He was able to elicit a vibrational response over a 100-1300 cm^{-1} range while Varnholt *et al.* focused on the 200-400 cm^{-1} region due to the limitations of the rolling circle filter cutoff at 170 cm^{-1} on the Scattered Circular Polarization-Raman Optical Activity (SCP-ROA) instrument and disinterest in the ligand vibrational range.¹⁶ The measured spectra was considered nontrivial since gold nanoclusters are considered weak scatters and absorb strongly in the visible region, hence the use of a 532 nm laser to carry out this study.¹⁶ A light intensity of 8 mW (milliwatts) was used while the sample was rotated at 3000 rpm to prevent excessive heating. They drew the conclusion that the type and number of thiolate ligands influence the spectrum and that there was a general shift to higher wavenumbers observed for more sterically demanding ligands.¹⁶

3.2.2 IR Vibrational Spectroscopy of AuNPs

There have been previous vibrational studies besides Raman Spectroscopy. Dolamic *et al.* studied gold clusters covered with 2-PET and characterized Au-S stretches around 300 cm^{-1} and below via far-infrared analysis.¹⁵ They reported slight shifting depending on the core size of the different clusters. The study analyzed 5 compounds $\text{Au}_{144}(\text{2-PET})_{60}$, $\text{Au}_{40}(\text{2-PET})_{24}$, $\text{Au}_{38}(\text{2-PET})_{24}$, $[\text{Au}_{25}(\text{2-PET})_{18}] \text{ TOA}$, and $[\text{Au}_{25}(\text{2-PET})_{18}]$. For reference TOA refers to the tetraoctylammonium counterion. They reported results of bands at 321 and 284 cm^{-1} in the spectral range for expected Au-S vibrations and associated a band near 490 cm^{-1} indicative of phenylethylthiolate conformation coupled to a C-C-S bending mode.¹⁵ They also utilized calculations performed by Tlahuice-Flores *et al.* to assign the tangential Au(staple)-S(staple) vibrations and Au(core)-S(staple) modes.²⁴

3.3 AuNP Core-Conversions

In previous works it has been shown that the Au-S interface is relatively flexible.¹⁶ This flexibility allows for the rearrangement of gold particles contained within the core as well as gold-thiol staple units. This staple rearrangement has been observed for various compounds such as $\text{Au}_{67}(\text{SR})_{35}$ to $\text{Au}_{36}(\text{SR})_{24}$ conversion as well as at elevated temperature conditions.^{28, 29} Additionally, adsorbed thiolates have been observed to “place-exchange” between different symmetry sites.³⁰ This is an intriguing quality that allows the gold core of the compound to undergo core-conversions to different compositions and number of atoms. This occurs by reacting a starter molecule with a physiochemically different thiol to induce a core-size conversion.²⁸ The ligand exchange and core-conversion can occur separately or simultaneously.²⁸ Rambukwella *et al.* demonstrated that $\text{Au}_{38}(\text{2-PET})_{24}$ is able to undergo a core-size reduction to $\text{Au}_{30}(\text{S-}t\text{Bu})_{18}$ via etching with *tert*-butylthiol with a $\text{Au}_{36}(\text{SCH}_2\text{CH}_2\text{Ph})_{24-x}(\text{S-}t\text{Bu})_x$ intermediate.²⁸ This reaction creates the compound coined “green-gold” by the Dass group due to its green appearance.²⁸

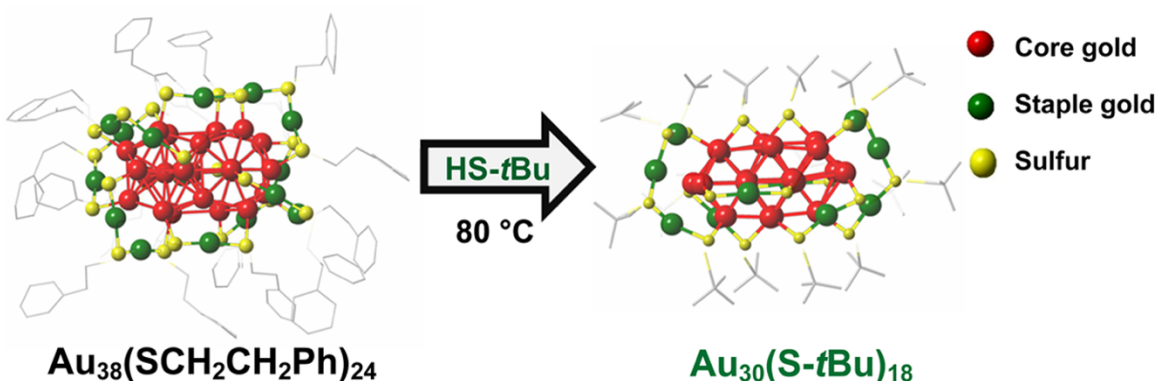


Figure 3.1 Visual depiction of the core-conversion process from $\text{Au}_{38}(\text{2-PET})_{24}$ geometry to $\text{Au}_{30}(\text{S-}t\text{Bu})_{18}$ geometry via etching with *tert*-butylthiol at 80°C .

Source: Milan Rambukwella, Luca Sementa, Alessandro Fortunelli, and Amala Dass, *The Journal of Physical Chemistry C* **2017** 121 (27), 14929-14935

Core conversions can result for a variety of reasons such as strong steric or electronic effects. In this reaction, the *tert*-butyl group of exchanging ligands exerts a strong steric effect upon the gold core, causing the core-size reduction to 30 gold atoms.²⁸ For the purposes of this paper, our interest lies in Au₃₀(S-*t*Bu)₁₈, first reported along with its crystal structure by the Dass group in 2013.³¹⁻³³ Au₃₀(S-*t*Bu)₁₈ has a sterically crowded thiolate ligand shell and similar core structures, such as Au₂₁ and Au₂₃, have been reported with similarly bulky thiolate ligands.²⁸ The Dass group reported that the core size is governed by the thiolate ligand shell, for example only Au₃₈ is stable with aliphatic and aliphatic-like ligands such as hexane thiol and phenylethane thiol, in contrast to that of the Au₃₀ core which is stable with bulkier ligands such as *tert*-butylthiol.²⁸

3.4 Geometric & Energetic Comparison of Au₃₈(2-PET)₂₄ and Au₃₀(S-*t*Bu)₁₈

There are several discriminating factors between the Au₃₈(2-PET)₂₄ and Au₃₀(S-*t*Bu)₁₈ samples. The Au₃₈(2-PET)₂₄ sample contains an Au₂₃ gold core while Au₃₀(S-*t*Bu)₁₈ sample contains a smaller Au₂₀ gold core.²⁸ Additionally, the Au-S interfaces also differ significantly. Au₃₈(2-PET)₂₄ contains three monomeric staple units and six dimeric staple units while Au₃₀(S-*t*Bu)₂₄ contains four monomeric staple units, two trimeric staples, and 2 bridging thiols.²⁸ These differences alongside the ligand exchange from 2-Phenylethelthiolate to *tert*-butylthiol and the core-conversion Au₃₆ intermediate species cause differences in the formation energy of the nanomolecules. The formation energies were investigated by comparison of the various specie's fragmentation energy, atomization energy, ligand shell separation, ionization potentials, electron affinities, and chemical hardness.

Rambukwella *et al.* noted that they expected to see similar covalent interactions since both ligands are considered aliphatic thiols; however, they reported that the S-H bond reaction energy in both the H-S-*t*Bu and H-SCH₂CH₂Ph were “nearly identical” having values of 4.86 eV for Au₃₈(2-PET)₂₄ and 4.87 eV for Au₃₀(S-*t*Bu)₁₈.²⁸ This result indicates that the chemical-behavioral differences between the compounds can be attributed to geometric or electronic effects due to the larger steric hindrance of the S-*t*Bu compound rather than Au-S covalent interactions.^{28, 40}

Rambukwella *et al.* reported that the formation energy was largest for Au₃₈(2-PET)₂₄, and therefore most stable due to the relative Au-S bond length caused by steric hindrance. The Au-S bond length ranges for Au₃₀(S-*t*Bu)₁₈ and Au₃₈(2-PET)₂₄ reported were 2.35-2.44 Å and 2.33-2.49 Å, respectively.²⁸

The atomization energy showed that Au₃₀(S-*t*Bu)₁₈ has preferable stability when compared to Au₃₈(2-PET)₂₄ Au-Au first-neighbor distance, which have values of 2.91 Å and 2.95 Å respectively.²⁸ It is also important to note that the staple units nearly detach due to steric hindrance in the Au₃₆(S-*t*Bu)₂₄ configuration.²⁸

Ligand shell separation analysis revealed that Au₃₈(2-PET)₂₄ has a very large ligand separation value dependent upon residual S-S binding; however, it is dominated by additional repulsion interactions between organic residues such as π - π bonding and T-Stacking of phenyl rings.^{28, 41}

Final comparisons indicated that Au₃₈(2-PET)₂₄ had higher ionization potential and electron affinities than Au₃₀(S-*t*Bu)₁₈; however, Au₃₀(S-*t*Bu)₁₈ demonstrated higher values than Au₃₈(2-PET)₂₄ for chemical hardness indicating that from an electrical standpoint, Au₃₀(S-*t*Bu)₁₈ is the more stable species.²⁸

Chapter 4: Raman Spectroscopic Comparison of Au₃₈(2-PET)₂₄ and Au₃₀(S-tBu)₁₈

4.1 Introduction

Thiolate gold nanoparticles have a very interesting electronic structure which allows atom clusters to behave more as molecules than coordination compounds as they have discrete optical transitions. They also have other properties such as fluorescence, which is useful for applications in bionanotechnology, making them excellent markers of electromagnetic radiation, which can be adjusted by altering the cluster size and ligand type.³⁴ Additionally, the protective shell of the gold-core can be altered for selective binding to enzyme and protein receptors, allowing their use as biosensors.³⁵ Gold nanoparticles are essentially a subdomain of colloids and surfaces and as such, they have often been in the limelight as the model system for these classes.³⁶ They possess unique properties, making them good heterogenous catalysts and for uses in size-dependent electrochemistry.³⁶ Additionally, high chemical stability makes them good candidates for analyzing self-assembled monolayers, biolabeling, DNA melting, and other applications.³⁶ Gold nanoparticles of 2 to 3 nm in diameter have been considered reactive for conjugation with proteins and DNA as well as with antibody Fc fragments used to identify tagged proteins in electron micrographs.³⁷

Furthermore, these compounds have a variety of applications in the biomedical field. They are often referred to as Nobel-metal nanoclusters, such as Au and Ag, that behave in similar ways to that of a quantum dot, as they require a single light source for stimulation of “different-emissive nanoclusters”.³⁸ Additionally, the wavelength of these clusters can be altered by changing the capping molecules and core size allowing for additional adaptability.³⁸ Due to these properties, there has been extensive investigation of the localized surface plasmon resonances. These utilize the interaction of several

nanoparticles' localized plasmon resonances and localized electromagnetic fields in coupled structures, allowing the detection of extremely small amounts of sample.³⁶ This technique is known as SERS. This signal enhancement was not necessary for the spectral imaging of these compounds as demonstrated by Varnholt *et al.*¹⁶ and Lemuel Tsang's spectral data.³⁹ In this study, we utilize classical Raman spectroscopy to compare the vibrational modes of Au₃₈(2-PET)₂₄ and its core-size reduction from bi-icosahedron to bicuboctahedron core geometry and ligand exchange to Au₃₀(S-tBu)₁₈ without the use of a temperature control stage for a previously, vibrationally unresearched nanoparticle cluster.²⁸

4.2 Methods

For this project, two thiolated gold nanoparticles were investigated; Au₃₈(2-PET)₂₄ and Au₃₀(S-tBu)₁₈. Both compounds were provided by Senthil Eswaramoorthy from the Dass group at the University of Mississippi and were characterized by UV-vis spectroscopy and MALDI spectrometry to confirm purity. Approximately 5 mg of sample was applied to a glass slide using dichloromethane. It is important to note that no methanol was used to lower the surface tension. The dichloromethane was then allowed to evaporate before any observations were made. All Raman spectroscopic data for this project was collected via a Horiba LabRAM HR Evolution. For both samples a 633 nm laser with an Ultra-Low Frequency (ULF) filter was used at 5% power, which translates to a power of approximately 699-736 μW , since 100% power often resulted in thermal degradation of the samples. A laser power measuring device, Laser Check by Coherent, was used to make these measurements. The Horiba's spectroscopic range is capable of reaching extremely low wavenumbers (5 cm^{-1}) utilizing the low frequency filter. A low of 100 cm^{-1} was

recorded for the $\text{Au}_{38}(\text{2-PET})_{24}$ sample and a low of 50 cm^{-1} was collected for the $\text{Au}_{30}(\text{S-tBu})_{18}$ due to large amounts of fluorescence in these lower wavenumber regions. The majority of $\text{Au}_{38}(\text{2-PET})_{24}$ spectra were collected with an acquisition time of 10 seconds and 20 accumulations without causing thermal degradation of the sample. The $\text{Au}_{30}(\text{S-tBu})_{18}$ sample spectra were collected using a maximum of 4 seconds of acquisition time for 10 accumulations, since a 5-second acquisition time caused thermal degradation of the $\text{Au}_{30}(\text{S-tBu})_{18}$ sample. It is important to note that no temperature control stage was used to acquire any data. Furthermore, a 600 gr/mm grating and 20x LWD objective was utilized to acquire all data. Prior to data collection for both samples, the Horiba Raman spectrometer was calibrated using the auto calibration feature with a fragment of silicon which has a characteristic peak at 520 cm^{-1} . Once the samples were placed under the microscope, data was collected at varying focuses. The lack of topographical features makes it challenging to properly focus on the sample surface. This is the reason the 633 nm laser was utilized over a 785 nm laser. It is also important to note that the spectrum proved extremely sensitive to focus, a characteristic also observed in Lemuel Tsang's thesis.³⁹ Wide wavenumber ranges of approximately $50\text{-}1300 \text{ cm}^{-1}$ were collected for both the $\text{Au}_{38}(\text{2-PET})_{24}$ and $\text{Au}_{30}(\text{S-tBu})_{18}$ samples. Ranges exhibiting characteristic peaks were focused on; such as 175-375, 600-900, and 960-1060 cm^{-1} for $\text{Au}_{38}(\text{2-PET})_{24}$ and 150-350, 575-700, 900-1100, and 1100-1300 cm^{-1} for $\text{Au}_{30}(\text{S-tBu})_{18}$.

4.3 Results & Discussion

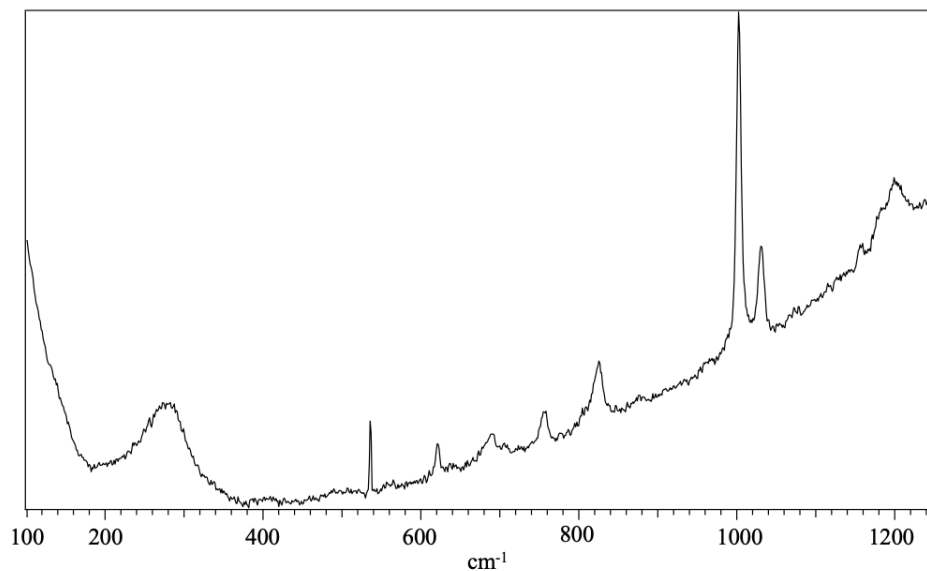


Figure 4.1 Raman spectrum of $\text{Au}_{38}(\text{2-PET})_{24}$ under 20x magnification with 633 nm ULF excitation from 100-1250 cm^{-1} . Notable Au-S characteristic peaks remain unresolved in the 200-400 cm^{-1} region. Other characteristic peaks appear at 540, 620, 690, 760, 825, 1000, 1030, and 1210 cm^{-1} .

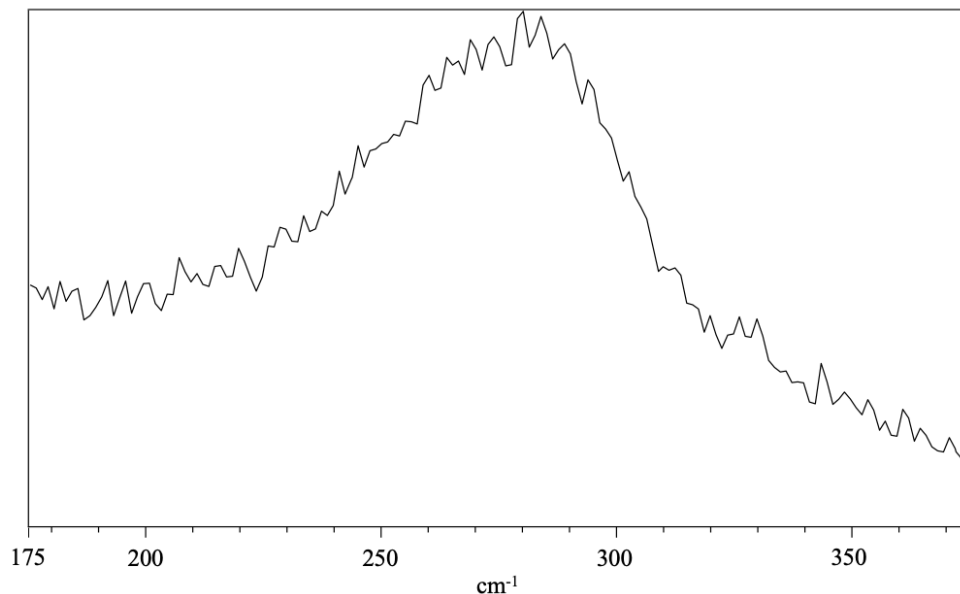


Figure 4.2 Raman spectrum of $\text{Au}_{38}(\text{2-PET})_{24}$ under 20x magnification with 633 nm ULF excitation from 175-375 cm^{-1} . Au-S stretches of the gold core commonly appear in this region, this region remains too unresolved to discriminate individual peaks.

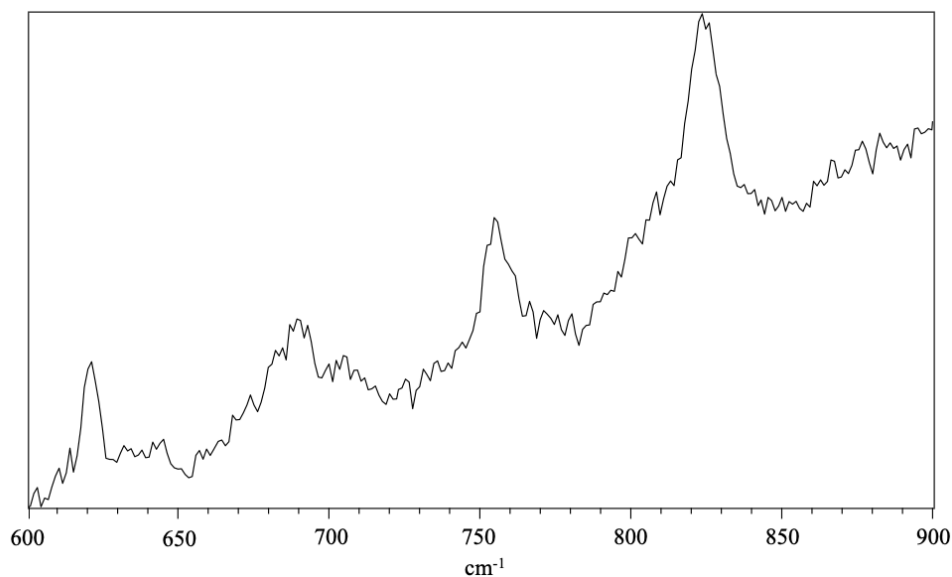


Figure 4.3 Raman spectrum of $\text{Au}_{38}(\text{2-PET})_{24}$ under 20x magnification with 633 nm ULF excitation from 600-900 cm^{-1} . Characteristic peaks appearing at 540, 620, 690, 760, and 825 cm^{-1} .

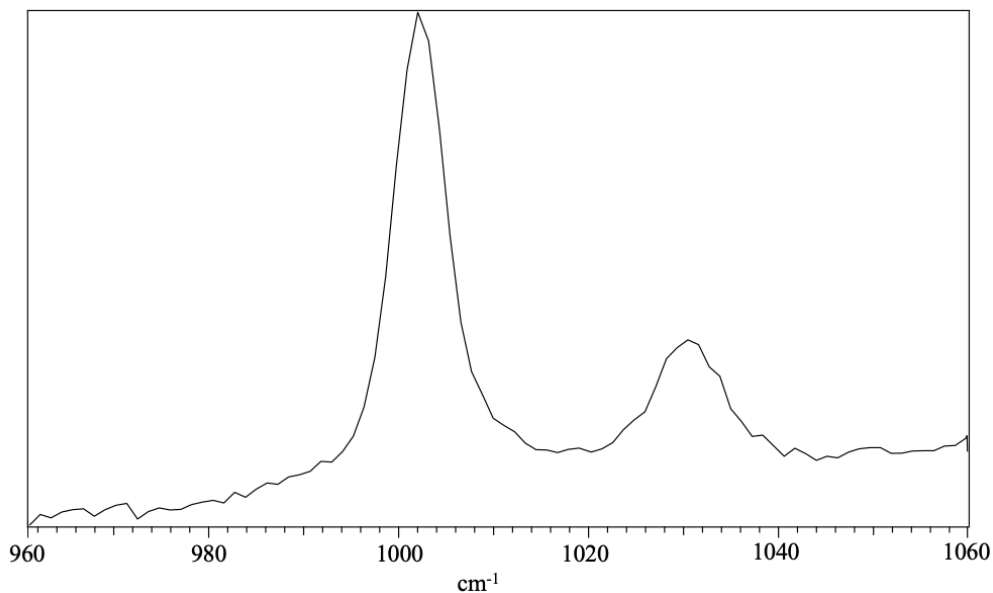


Figure 4.4 Raman spectrum of $\text{Au}_{38}(\text{2-PET})_{24}$ under 20x magnification with 633 nm ULF excitation from 960-1060 cm^{-1} . Characteristic ligand peak of phenylethylthiolate appears at 1000 cm^{-1} and is attributed to a combination of C-H ring bending and wagging modes due to assignment from previous works.¹⁶

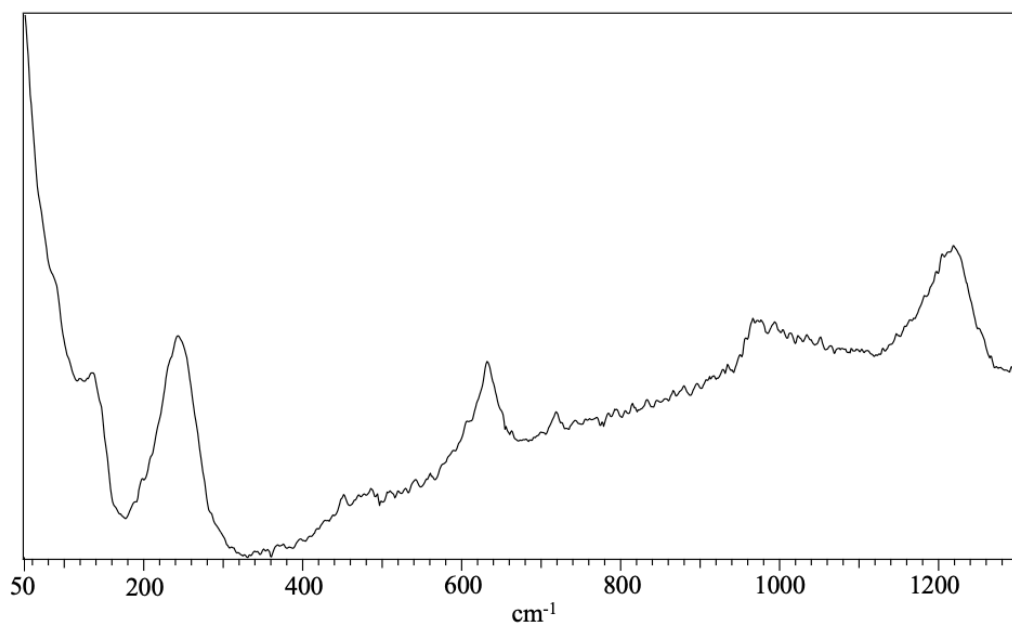


Figure 4.5 Raman spectrum of $\text{Au}_{30}(\text{S-tBu})_{18}$ under 20x magnification with 633 nm ULF from 50-1300 cm^{-1} . We believe there has been no previous vibrational study performed on $\text{Au}_{30}(\text{S-tBu})_{18}$, which appears to have characteristic peaks at 250, 636, 975, and 1220

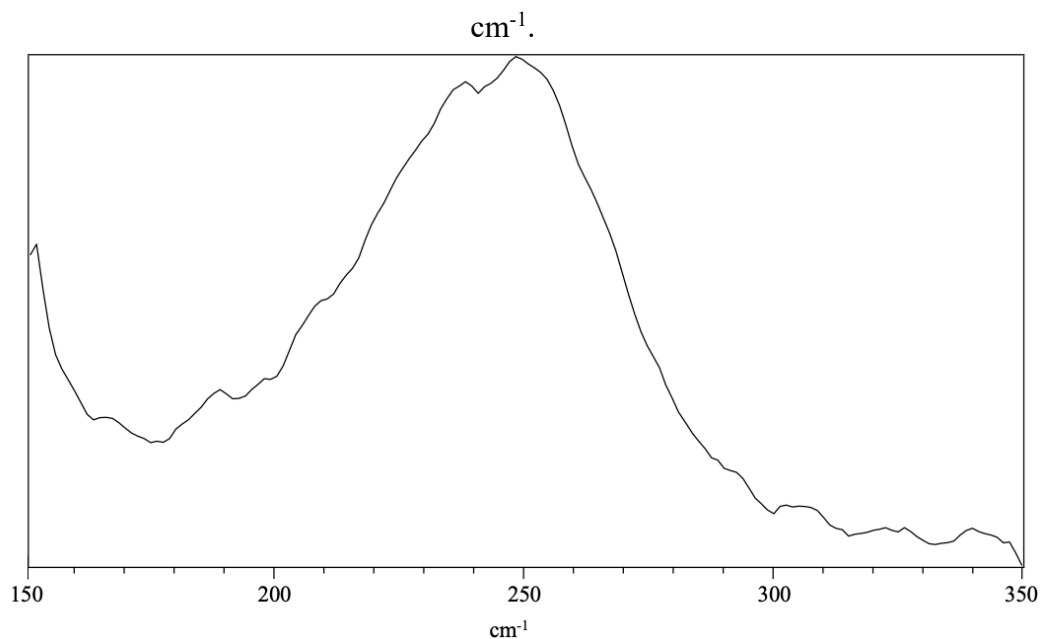


Figure 4.6 Raman spectrum of $\text{Au}_{30}(\text{S-tBu})_{18}$ under 20x magnification with 633 nm ULF excitation from 150-350 cm^{-1} . This peak could be attributed to Au-S stretching, common for these compounds in this region. This sharp peak in 200 cm^{-1} range is likely an

unresolved region of Au-S stretches; however, resolution of this region remains insufficient to differentiate the individual peaks.^{15, 16}

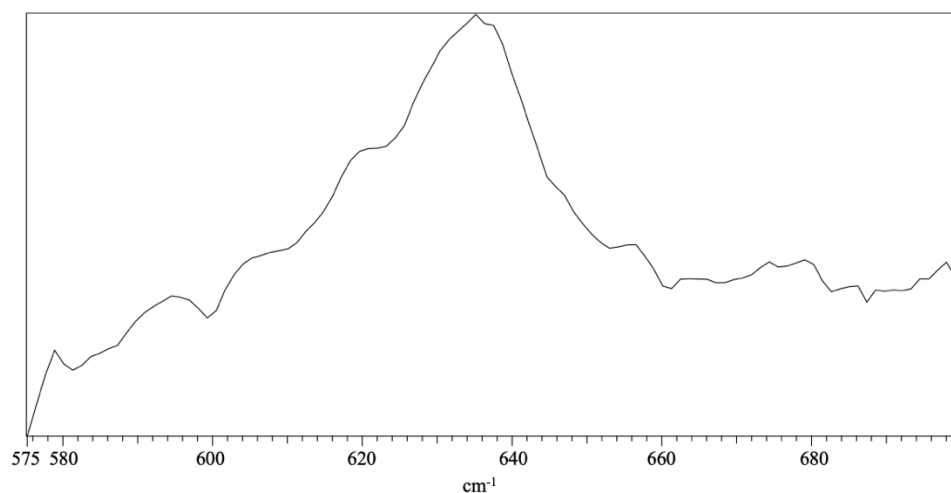


Figure 4.7 Raman spectrum of $\text{Au}_{30}(\text{S-tBu})_{18}$ under 20x magnification with 633 nm ULF excitation from 575-700 cm^{-1} .

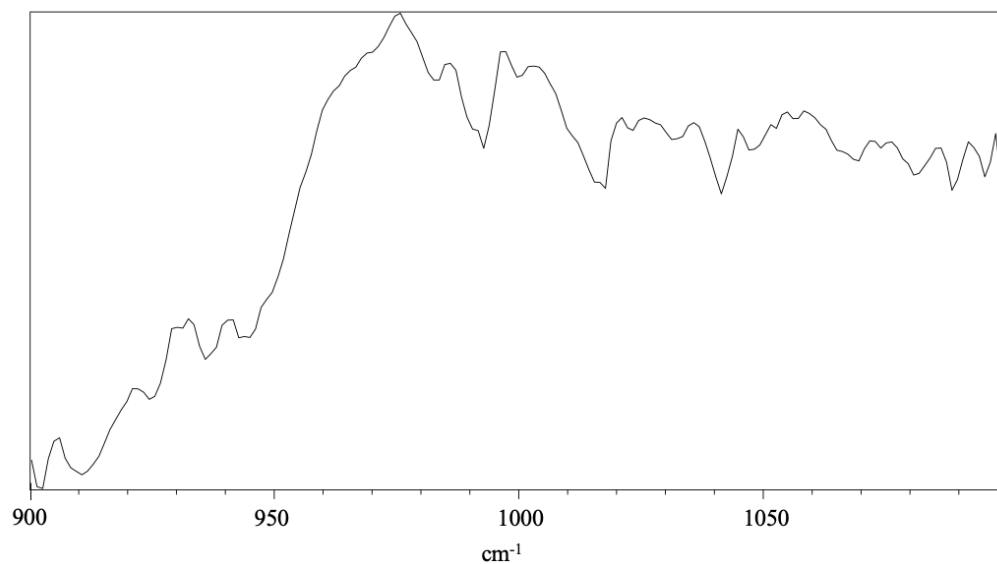


Figure 4.8 Raman spectrum of $\text{Au}_{30}(\text{S-tBu})_{18}$ under 20x magnification with 633 nm ULF excitation from 900-1100 cm^{-1} .

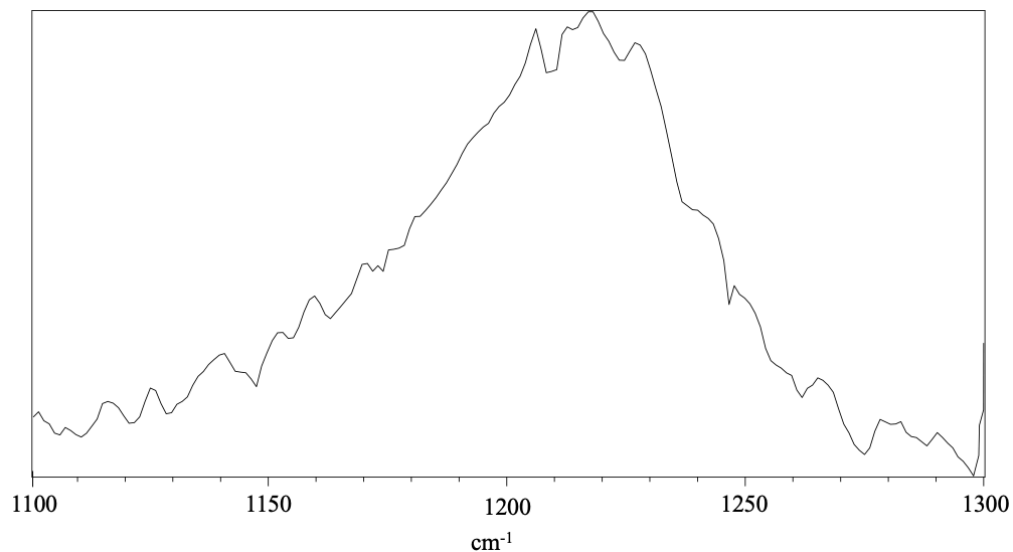


Figure 4.9 Raman spectrum of $\text{Au}_{30}(\text{S-tBu})_{18}$ under 20x magnification with 633 nm ULF excitation from 1100-1300 cm^{-1} .

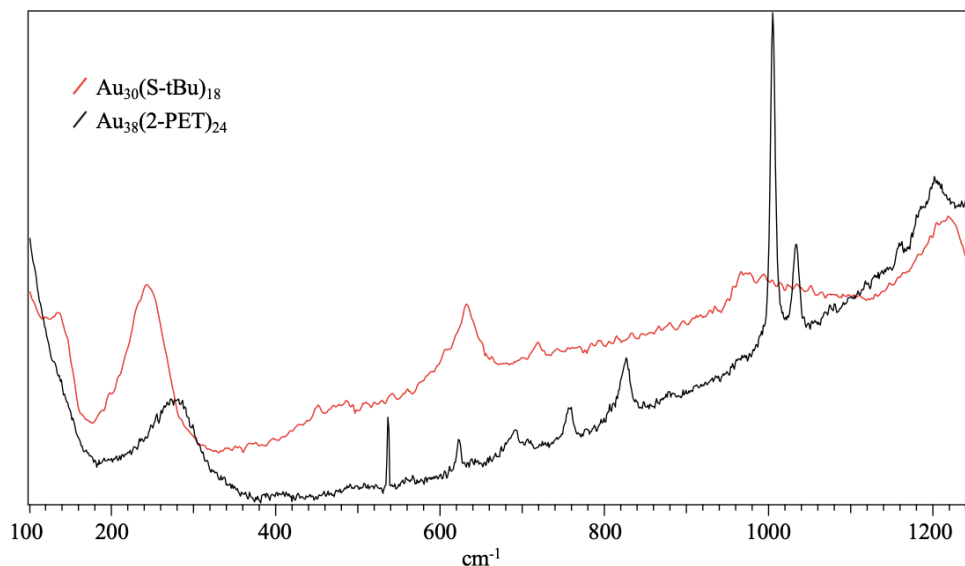


Figure 4.10 Raman spectral comparison of $\text{Au}_{38}(\text{2-PET})_{24}$ and $\text{Au}_{30}(\text{S-tBu})_{18}$ samples under 20x magnification with 633 nm ULF excitation from 100-1250 cm^{-1} .

After etching with *tert*-butylthiol, $\text{Au}_{38}(\text{2-PET})_{24}$ undergoes a core-size reduction to an $\text{Au}_{36}(\text{SCH}_2\text{CH}_2\text{Ph})_{24-x}(\text{S-tBu})_x$ intermediate followed by conversion to bi-cuboctahedron geometry, $\text{Au}_{30}(\text{S-tBu})_{18}$. This new core-conversion structure was studied

for the first time via Raman spectroscopy and was found to have characteristic peaks in the 200-300 cm^{-1} region, likely due to the various Au-S stretching modes. Though this region remains too unresolved to identify individual peaks, we observed that the spectral range for Au-S stretching modes of the $\text{Au}_{30}(\text{S-tBu})_{18}$ sample is smaller than the previously assigned 200-400 cm^{-1} range of the Au-S stretching modes for $\text{Au}_{38}(\text{2-PET})_{24}$.^{15, 16} These vibrations, consisting of Au-S-C bending, Au-S-C bending of monomeric and dimeric staples, symmetric stretching of monomeric staples, radial vibrations of outer sulfurs of dimeric staple units, radial vibration of central sulfurs of dimeric staple units, and tangential vibrations should appear at 178, 208, 257, 286, 316, and 357 cm^{-1} respectively, according to assignments from previous works.¹⁶ Furthermore, the low wavenumber peaks of $\text{Au}_{30}(\text{S-tBu})_{18}$, supposedly associated with Au-S stretching modes, has a maximum intensity occurring at approximately 250 cm^{-1} . This is in contrast to the Au-S stretching modes of $\text{Au}_{38}(\text{2-PET})_{24}$ that occur around 280 cm^{-1} and are likely associated with radial vibrations of the central sulfur atom located on the long staples which have been previously assigned.¹⁶ Additionally, we observed some characteristic peaks on the Raman spectrum of the $\text{Au}_{38}(\text{2-PET})_{24}$ sample around 1000 and 1210 cm^{-1} consistent with C-H ring bending and wagging modes of the ligand, 2-phenylethylthiol, also assigned in previous works.¹⁶ Given that these are ligand-specific vibrations, when compared to the $\text{Au}_{30}(\text{S-tBu})_{18}$ spectra illustrated in Figure 4.10, the absence of the 1000 cm^{-1} peak is expected. Despite the ligand exchange from 2-PET to *tert*-butylthiol, a similar peak to that of the 1210 cm^{-1} in $\text{Au}_{38}(\text{2-PET})_{24}$ was observed for the $\text{Au}_{30}(\text{S-tBu})_{18}$ sample at approximately 1220 cm^{-1} ; however, this remains uncharacterized. Additionally, there was no peak detected at 1030 cm^{-1} for the $\text{Au}_{30}(\text{S-tBu})_{18}$ sample.

4.4 Summary

With this project we were able to successfully investigate the variance in the vibrational modes of $\text{Au}_{38}(\text{2-PET})_{24}$ before and after conversion to a bi-cuboctahedron core geometry known as $\text{Au}_{30}(\text{S-tBu})_{18}$ / “green-gold” via Raman spectroscopy. This shows the sensitivity of the spectrum to key changes in AuNP core structure and aids in the characterization of new vibrational modes for previously unobserved $\text{Au}_{30}(\text{S-tBu})_{18}$. While the individual plasmon modes of both $\text{Au}_{38}(\text{2-PET})_{24}$ and $\text{Au}_{30}(\text{S-tBu})_{18}$ remain unresolved, a generalized shift in the 200-400 to 200-300 cm^{-1} regions was observed, suggesting $\text{Au}_{30}(\text{S-tBu})_{18}$ allows for less Au-S stretching modes to develop, possibly due to steric hindrance. For future studies, a temperature control stage could be utilized to investigate AuNP vibrational modes for longer acquisitions and for a greater number of accumulations as well as higher laser powers. This is especially important for $\text{Au}_{30}(\text{S-tBu})_{18}$ as the sample appeared more susceptible to localized heating than the $\text{Au}_{38}(\text{2-PET})_{24}$ sample. Here we can see the comparative nature of spectra for thiolated gold nanoparticles undergoing a core-size reduction via ligand exchange pathways. Despite some of the masking of upper wavenumber region characteristics by fluorescence and lower wavenumber resolution, these spectral differences provide researchers with valuable insight into the molecular like properties of AuNPs undergoing core-conversions. Additional planned experiments were not possible due to the COVID-19 national disaster.

dChapter 5: Supplemental Information

5.1 Experimental Setup & Methodologies

One of the most important factors for collecting AuNP data is using a relatively freshly synthesized sample, whether for the $\text{Au}_{38}(\text{2-PET})_{24}$ or $\text{Au}_{30}(\text{S-tBu})_{18}$ samples. Figure 5.1, shown below, illustrates the difference in spectra obtained for an approximately 7-year-old sample of $\text{Au}_{30}(\text{S-tBu})_{18}$ (right) versus a less than 3-year-old sample of $\text{Au}_{30}(\text{S-tBu})_{18}$ (left). The spectral features are noticeably more pronounced in the newer sample despite using the same methodology to collect data.

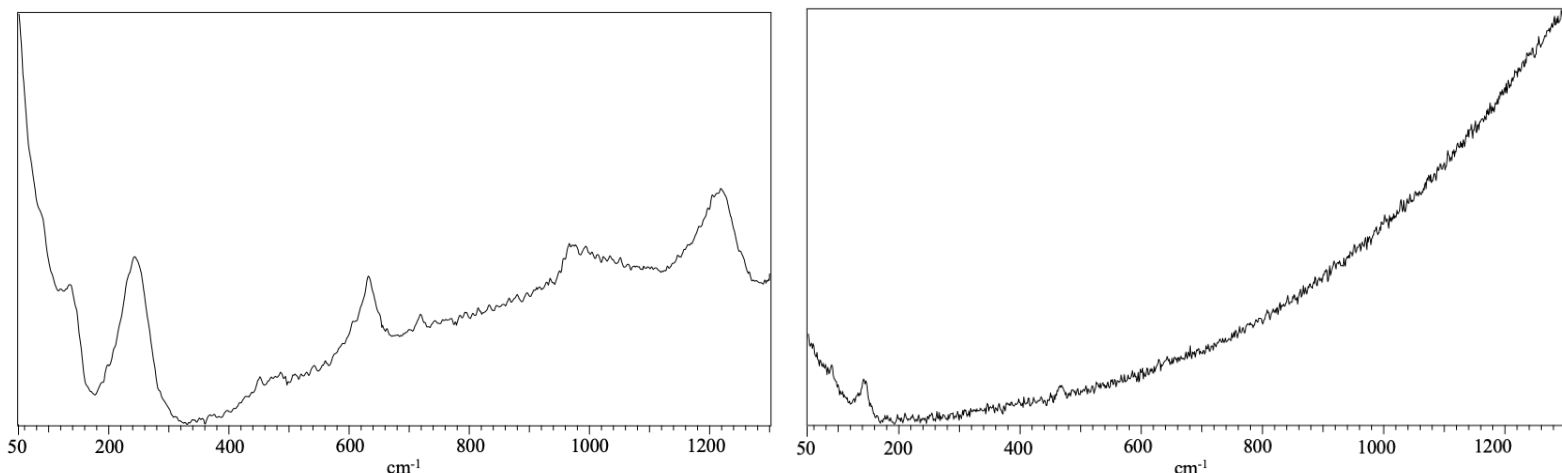


Figure 5.1 Raman spectrum of $\text{Au}_{30}(\text{S-tBu})_{18}$ under 20x magnification with 633 nm ULF excitation from 50-1300 cm^{-1} . This shows the comparison of a fresh 3-year-old sample (left) and a degraded 7-year-old sample (right).

When preparing the samples with dichloromethane, the entirety of the synthesized sample was placed in approximately 1-3 mL of dichloromethane to ensure the maximum concentration of the sample. High concentrations are useful because the sample will need to be located on the slide under the Raman microscope, and larger particles can be found with ease. After allowing the dichloromethane to evaporate from the sample slide, locate

the particle on the glass slide utilizing a low power objective (10x), then proceed to collect data using a higher power objective (20x).

Since the topographical features of these compounds are not well defined, focusing on the sample will require trial and error. Once an area of the sample is selected, short collection times should be used, such as an acquisition time of 4 seconds with 5-10 accumulations. This will provide a general overview of the spectral features of the samples, and the signal to noise ratio can be adjusted by adjusting the focus. This collection provides more spectral information on the sample than the real-time-display feature. After obtaining spectra, continue to adjust the focus to maximize the samples spectral response/intensity and proceed to collect data with higher acquisition times and accumulations.

A 633 nm laser was used over a 532 nm laser because the 532 nm, even at lower laser powers, resulted in degradation of the samples due to its higher energy. Additionally, the 633 nm was used over a 785 nm laser since the 785 nm starts to go outside of the visible spectrum of light. Therefore, it becomes more difficult to focus the light source on the sample as when the image is focused; the laser will be slightly out of focus and vice versa; however, proper focusing can be achieved through additional trial and error.

Due to localized heating susceptibility, data could not be collected at 100% power with the 633 nm laser. 1% laser power was too low to elicit any kind of discernable spectral features for either of the samples. For this reason, 5% power was utilized to capture the spectral features of both the $\text{Au}_{38}(\text{2-PET})_{24}$ and $\text{Au}_{30}(\text{S-tBu})_{18}$ samples. For the sake of reproducibility, 5% power of the 633 nm He/Ne laser with the ULF filter installed translated to powers of approximately 699-736 μW . For the $\text{Au}_{38}(\text{2-PET})_{24}$ sample, 5% laser power began to cause thermal degradation above an acquisition time of 10 seconds with 20 accumulations and above an acquisition time of 4 seconds with 10 accumulations

for the $\text{Au}_{30}(\text{S-tBu})_{18}$ sample. Therefore, the $\text{Au}_{30}(\text{S-tBu})_{18}$ sample appeared slightly more susceptible to thermal degradation than the $\text{Au}_{38}(\text{2-PET})_{24}$ sample.

A 600 gr/mm grating was utilized for all data collected in this project. Higher spectral resolutions could be obtained by recording excitation with the 633 nm laser over a smaller wavenumber range. Additionally, an 1800 gr/mm grating could be utilized to achieve higher spectral resolutions; unfortunately, these tests could not be performed due to the COVID-19 national disaster.

List of References:

- 1) Greiner, W. *Quantum Mechanics: An Introduction*, **2001**.
- 2) Frary, M. *The World of Electricity (1820-1904)*. International Electrotechnical Commission, **2020**.
- 3) Le Ru, E. C.; Etchegoin, P. G. *Principles of Surface-Enhanced Raman Spectroscopy and related plasmonic effect*, **2009**.
- 4) Atkins, P.; Friedtman, R. *Molecular Quantum Mechanics*, **2005**.
- 5) Tudos, A. K.; Shasfoot, R. *Handbook of Surface Plasmon Resonance*, **2008**.
- 6) Jackson, J. D. *Classical Electrodynamics*, **1998**.
- 7) Karhaman, M. *Fabrication and Characterization of Flexible and Tunable Plasmonic Nanostructures*, **2013**.
- 8) Sharma, B., *SERS: Materials, applications and the future*, **2012**.
- 9) Smekal, A. *Zur Quantentheorie der Dispersion*, **1923**.
- 10) Raman, C. V. *A new radiation* Indian Journal of Physics, **1928**.
- 11) Andor, *What Are the Basic Principles of Raman Spectroscopy?* Oxford Instruments, **2020**.
- 12) Robinson, J.W.; Skelly Frame, E.M.; Frame II, G.M. *Undergraduate Instrumental Analysis*, **2005**.
- 13) Granger, R. M.; Yochum, H. M.; Granger, J. N.; Sienerth, K. D. *Instrumental Analysis*, **2017**.
- 14) Jadzinsky, P.D., G. Calero, C. J. Ackerson, D. A. Bushnell and R. D. Kornberg, Structure of a Thiol Monolayer-Protected Gold Nanoparticle at 1.1 Å Resolution. *Science*, 2007. **318**, p. 430-433.

- 15) I. Dolamic, B. Varnholt and T. Bürgi, *Phys. Chem. Chem. Phys.*, 2013, **15**, 19561—19565
- 16) Birte Varnholt, Patric Oulevey, Sandra Luber, Chanaka Kumara, Amala Dass, and Thomas Bürgi. *The Journal of Physical Chemistry C* **2014** *118* (18), 9604-9611
- 17) Murray, R. W. Nanoelectrochemistry: Metal Nanoparticles, Nanoelectrodes, and Nanopores. *Chem. Rev.* **2008**, 108, 2688–2720.
- 18) Wang, L.-M.; Wang, L.-S. Probing the Electronic Properties and Structural Evolution of Anionic Gold Clusters in the Gas Phase. *Nanoscale* **2012**, *4*, 4038–4053.
- 19) Dass, A. Nano-Scaling Law: Geometric Foundation of Thiolated Gold Nanomolecules. *Nanoscale* **2012**, *4*, 2260–2263.
- 20) Walter, M.; Akola, J.; Lopez-Acevedo, O.; Jadzinsky, P. D.; Calero, G.; Ackerson, C. J.; Whetten, R. L.; Gronbeck, H.; Hakkinen, H. A Unified View of Ligand-Protected Gold Clusters as Superatom Complexes. *Proc. Natl. Acad. Sci. U. S. A.* **2008**, 105, 9157–9162.
- 21) J. C. Love, L. A. Estroff, J. K. Kriebel, R. G. Nuzzo and G. M. Whitesides, *Chem. Rev.*, 2005, **105**, 1103–1169.
- 22) H. Hakkinen, *Nat. Chem.*, 2012, **4**, 443–455.
- 23) M. A. Reed, C. Zhou, C. J. Muller, T. P. Burgin and J. M. Tour, *Science*, 1997, **278**, 252–254.
- 24) Tlahuice-Flores, A.; Whetten, R. L.; Jose-Yacamán, M. Vibrational Normal Modes of Small Thiolate-Protected Gold Clusters. *J. Phys. Chem. C* **2013**, *117*, 12191–12198.

- 25) Price, R. C.; Whetten, R. L. Raman Spectroscopy of Benzenethiolates on Nanometer-Scale Gold Clusters. *J. Phys. Chem. B* **2006**, 110, 22166–22171.
- 26) Parker, J. F.; Choi, J.; Wang, W.; Murray, R. W. Electron Self-Exchange Dynamics of the Nanoparticle Couple $[\text{Au}_{25}(\text{SC}_2\text{Ph})_{18}]^{0/1-}$ by Nuclear Magnetic Resonance Line-Broadening. *J. Phys. Chem. C* **2008**, 112, 13976–13981.
- 27) M. Farrag, M. Tschurl, A. Dass and U. Heiz, *Phys. Chem.*, 2013, 15, 12539–12542.
- 28) Milan Rambukwella, Luca Sementa, Alessandro Fortunelli, and Amala Dass, *The Journal of Physical Chemistry C* **2017** 121 (27), 14929-14935
- 29) Nimmala, P. R.; Dass, A. $\text{Au}_{36}(\text{SPh})_{23}$ Nanomolecules. *J. Am. Chem. Soc.* **2011**, 133, 9175–9177.
- 30) Beqa, L.; Deschamps, D.; Perrio, S.; Gaumont, A.-C.; Knoppe, S.; Bürgi, T. Ligand Exchange Reaction on $\text{Au}_{38}(\text{SR})_{24}$, Separation of $\text{Au}_{38}(\text{SR})_{23}(\text{SR}')_1$ Regioisomers, and Migration of Thiolates. *J. Phys. Chem. C* **2013**, 117, 21619–21625.
- 31) Crasto, D.; Dass, A. Green Gold: $\text{Au}_{30}(\text{S-t-C}_4\text{H}_9)_{18}$ Molecules. *J. Phys. Chem. C* **2013**, 117, 22094–22097.
- 32) Crasto, D.; Malola, S.; Brosofsky, G.; Dass, A.; Häkkinen, H. Single Crystal Xrd Structure and Theoretical Analysis of the Chiral $\text{Au}_{30}\text{S}(\text{S-t-Bu})_{18}$ Cluster. *J. Am. Chem. Soc.* **2014**, 136, 5000–5005.
- 33) Dass, A.; et al. Crystal Structure and Theoretical Analysis of Green Gold $\text{Au}_{30}(\text{S-tBu})_{18}$ Nanomolecules and Their Relation to $\text{Au}_{30}\text{S}(\text{S-tBu})_{18}$. *J. Phys. Chem. C* **2016**, 120, 6256–6261.

- 34) Aubin-Tam, M. E., and Hamad-Schifferli, K. (2005) Gold nanoparticle-cytochrome C complexes: the effect of nanoparticle ligand charge on protein structure. *Langmuir* 21, 12080–12084.
- 35) Y. Negishi, Y. Takasugi, S. Sato, H. Yao, K. Kimura and T. Tsukuda, “Magic-numbered Au-n clusters protected by glutathione monolayers (n=18, 21, 25, 28, 32, 39): isolation and spectroscopic characterization,” *J. Am. Chem. Soc.*, 126: 6518-6519, **2004**.
- 36) Rajesh Sardar, Alison M. Funston, Paul Mulvaney, and Royce W. Murray, *Langmuir*, **2009** 25 (24), 13840-13851
- 37) Christopher J. Ackerson, Pablo D. Jadzinsky, Jonathan Z. Sexton, David A. Bushnell, and Roger D. Kornberg, *Bioconjugate Chemistry*, **2010** 21 (2), 214-218
- 38) Lin, C.; Lee, C.; Hsieh, J.; Wang, H.; Li, J.; Shen, J.; Chan, W.; Yeh, H.; Chang, W. H., *Journal of Medical and Biological Engineering*, **2009** 29 (6), 276-283
- 39) Tsang, L. (2017). *Raman Spectroscopic Studies of Novel Gold-Containing Nanomaterials* (Unpublished master’s thesis). University of Mississippi, Oxford, Mississippi, United States.
- 40) Jung, J.; Kang, S.; Han, Y.-K. Ligand Effects on the Stability of Thiol-Stabilized Gold Nanoclusters: Au₂₅(SR)₁₈⁻, Au₃₈(SR)₂₄, and Au₁₀₂(SR)₄₄. *Nanoscale* **2012**, 4, 4206–4210.
- 41) Nimmala, P. R.; Theivendran, S.; Barcaro, G.; Sementa, L.; Kumara, C.; Jupally, V. R.; Apra, E.; Stener, M.; Fortunelli, A.; Dass, A. Transformation of Au₁₄₄(SCH₂CH₂Ph)₆₀ to Au₁₃₃(SPh-tBu)₅₂ Nano- molecules: Theoretical and Experimental Study. *J. Phys. Chem. Lett.* **2015**, 6, 2134–2139.

